Nuclear Instruments and Methods in Physics Research A324 (1993) 145–155
North-Holland

NUCLEAR
INSTRUMENTS
& METHODS
IN PHYSICS
RESEARCH
Section A

# A setup for precise measurements of scintillating fiber bundles using an optoelectronic readout chain and a silicon microstrip detector system

J. Bähr, A. Bischoff, K. Hiller [1], B. Hoffmann, W. Lange, H. Lüdecke, R. Nahnhauer, W.D. Nowak, M. Pohl, H.E. Roloff and K. Sulanke
*DESY-IfH Zeuthen, Platanenallee 6, O-1615 Zeuthen, Germany*

J.P. Fabre, B. Friend, W. Flegel, J. Panman, S. Reynaud, G. Stefanini and K. Winter
*CERN, Geneva, Switzerland*

M. Gruwe [2] and Ch. Mommaert [3]
*Interuniversity Institute for High Energies (ULB-VUB), Brussels, Belgium*

Received 24 July 1992

A setup designed for the investigation of the properties of coherent scintillating fiber bundles and ribbons is described in some detail. The fiber readout is realized by a three stage image intensifier chain and a CCD matrix. A silicon strip detector telescope defines a precise reference system. The results of first measurements in a 5 GeV/$c$ hadron beam at the CERN proton synchrotron demonstrate the capabilities of the apparatus.

## 1. Introduction

The use of scintillating fibers in future particle physics detectors is presently widely under discussion [1,2]. Applications were designed for high resolution targets, tracking detectors, particle identification and calorimetry [3–6]. First experimental experience looks promising [5]. However, further optimisation of fiber parameters and readout components seems possible and worthwhile.

During the last years several groups tried to develop scintillating fibers with high light output and low light attenuation [7–11]. This development implies high statistics studies of single fibers, fiber ribbons and bundles with minimum ionizing particles, which are preferably done using particle beams at accelerators. Because the final parameters of a fiber detector are influenced by the properties of the fiber array as well as those of the readout device, careful studies are necessary to find an optimal combination.

In the following we describe a test beam setup developed for measurements of fiber targets of up to ~ 1 m length. They consist of scintillating fibers which are arranged in coherent bundles with cross sections of up to a few cm$^2$. The basic idea is to compare the fiber target hit patterns with tracks precisely predicted from a silicon microstrip detector telescope. In this way one gets information about the hit density, the attenuation length, and the resolution of the fiber target from an independent measuring system.

In section 2 we give an overview of the detector layout. Section 3 contains the description of the optoelectronic readout chain. The parameters of the silicon microstrip telescope are discussed in section 4. The trigger scheme and the on-line data acquisition are described briefly in section 5. In a first methodical run, different fiber and capillary targets were investigated in a 5 GeV/$c$ negative hadron beam at the CERN proton synchrotron. Results of this run are presented in section 6 to demonstrate the capabilities of the setup. Finally, some conclusions are drawn.

## 2. Detector layout

A schematical view of the setup is given in fig. 1. The fiber target is mounted on a scanner bench with the optoelectronic readout chain, including parts of the

[1] Presently research associate at CERN.
[2] Institut de Recherche Scientifique pour l'Industrie et l'Agriculture.
[3] Inter-University Institute for Nuclear Science.

0168-9002/93/$06.00 © 1993 – Elsevier Science Publishers B.V. All rights reserved

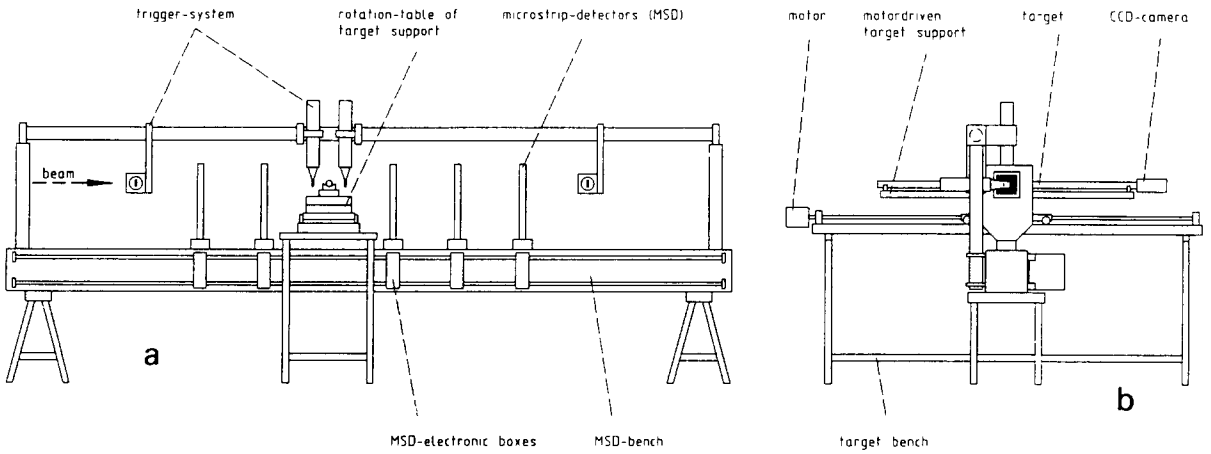


Fig. 1. The setup: the fiber target with the CCD camera on the target bench, the silicon microstrip detector telescope and the trigger counters on the steel bench. (a) Sideview. (b) frontfiew

front-end electronics. This scanner bench can be moved in steps of 1 cm up to a maximum distance of 1.2 m by remote control. Because some target parameters, e.g. the hit density, are quite different for particles traversing the target longitudinally or transversely with respect to the fiber axis, the scanner bench can be fully rotated in the horizontal plane.

The silicon microstrip telescope is mounted on a stable steel bench of 2.7 m length which can be aligned with respect to the beam by several bolts. The telescope consists of five detectors each measuring two coordinates. The two planes of each microstrip detector are installed in a metallic frame (paddle). Two paddles are positioned in front of the target and three behind. The minimum distance between two paddles, because of their mechanical fixation on the steel bench, is about 10 cm. Their positions are chosen according to the different target sizes and orientations. To minimize the influence of multiple Coulomb scattering on the track prediction inside the fiber target the paddles were placed as close as possible to the target.

The steel bench carries also the trigger system consisting of four scintillation counters. The trigger counters are freely movable along the bench so that fiber targets of different size and orientation may be used. They can be combined differently to obtain trigger

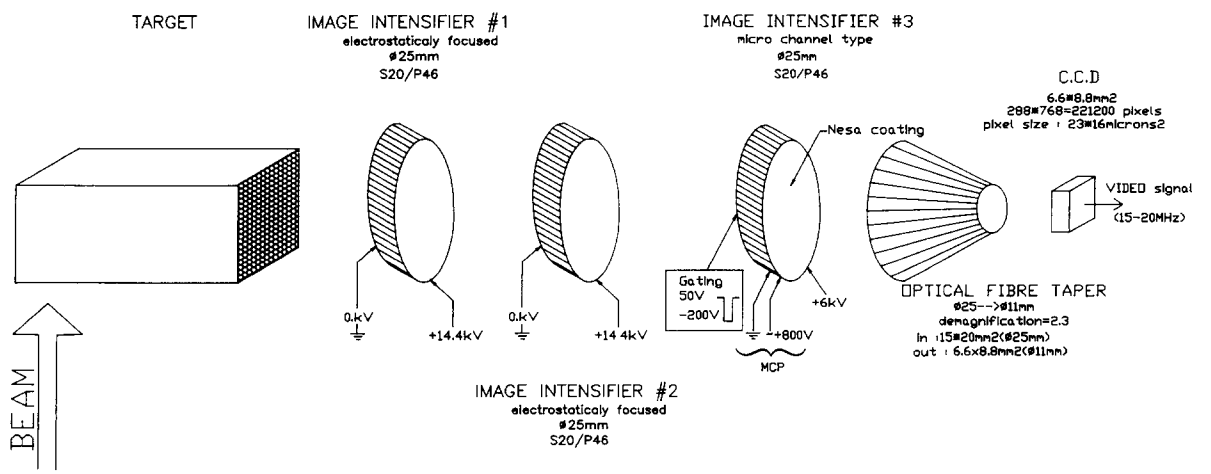


Fig. 2. The scheme of the optoelectronic readout chain: the first two stages are electrostatically focused image intensifiers, the third stage is a proximity focused one with a microchannel plate. A passive fiber taper couples the 25 mm diameter output window to the CCD.

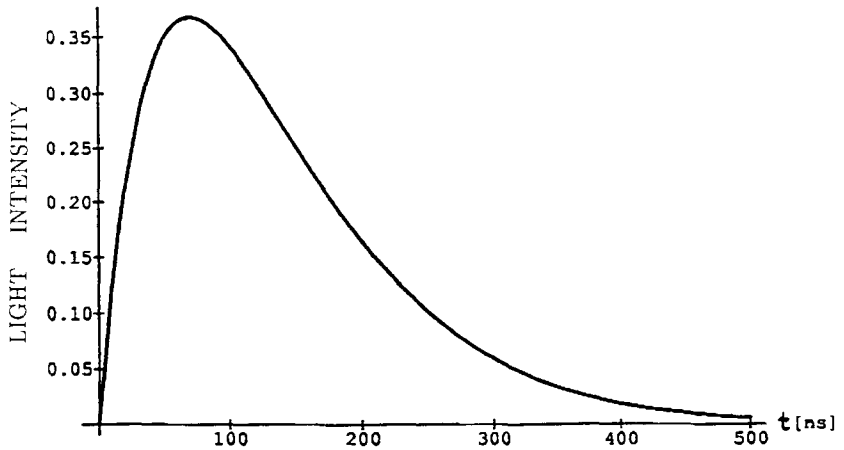


Fig. 3. The time dependence of a light signal due to the first two image intensifier stages with P46 phosphor screens Light reaching the third stage can be gated by the delayed signal produced by the trigger counters.

conditions for single beam tracks or interactions inside the fiber target.

### 3. The optoelectronic readout chain

The light signal arising from a charged particle traversing the scintillating fibers or capillaries is amplified in the optoelectronic readout chain which consists of three coupled image intensifiers (II). The amplified image is subsequently detected on a charge-coupled device (CCD). The analogue output of the CCD is digitised by an image processing port (IPP), which allows filtering and storing of the data.

The first two IIs are electrostatically focused [#1], while the third stage is a proximity focused II containing a microchannel plate (MCP) [#2]. The combination of the three IIs in the optoelectronic readout chain is sketched in fig. 2. Each II has a photocathode at the entrance window and a phosphor screen at the output window. An incoming photon impinges onto the photocathode and may liberate an electron which is then accelerated in a strong electric field. Hitting the phosphor screen the electron produces an amplified light signal. The light amplification (gain) of an electrostatically focused II depends mainly on the cathode–anode voltage and the phosphor material.

All IIs are equipped with S20 photocathodes and fast P46 phosphor screens. The electrostatically focused II have a quantum efficiency of 16.2 and 19.5%, respectively. Their gain is 7 photons per photon for a nominal voltage of 14.4 kV. The third II is characterized by a gain of about 1000 owing to the multiplication of electrons in the microchannel plate which is between the photocathode and the phosphor screen. The intense electron multiplication arises from secondary electron emission on the channel walls. The potential between the faces of the MCP is set to an adjustable voltage of about 800 V which dictates the gain of the chain. Leaving the MCP, the electron cascade is accelerated by a voltage of 6 kV before it hits the phosphor screen. The gating of the chain is done by changing the voltage of the third II photocathode with respect to the MCP input face. It is opened by setting this photocathode to $-200$ V while a slightly positive voltage closes it. The optical memory needed for the trigger decision is provided by the decay time of the phosphors of the IIs which are in front of the MCP. The P46 phosphor has a decay time of $\sim 70$ ns and the combined time characteristics of the first two IIs is shown in fig. 3.

All three IIs have an entrance and output window of 25 mm diameter. A subsequent fiber optical taper reduces the image to 11 mm diameter which matches the size of the CCD. The intrinsic spatial resolutions are 17, 14 and 28 μm for the first, second and third II, respectively.

The electrostatically focused IIs are characterized by nonnegligible image distortions. To measure the distortion some images of a well-known quadratic grid were stored and analysed. An image of the grid is shown in fig. 4. Obviously, the overall demagnification of an image is not constant over the sensitive area of the chain. Assuming a radially symmetric demagnification $D$, it can be described by the formula

$$D = D_0 + D_2 \times R^2,$$

[#1] Delft Electronische Producten, P.O. Box 60, Dwazziewegen 2, 9300 AB Roden, Netherland.

[#2] Proxitronic, Robert-Bosch-Str. 34, D-6140 Bensheim, Germany.

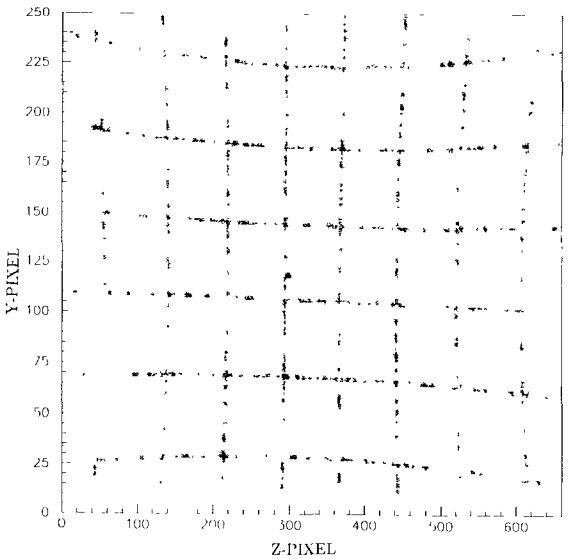


Fig. 4. The pixel image of a regular quadratic grid distorted by the electrostatically focused stages of the image intensifier chain. The distortion can be described by a dependence of the demagnification on the distance to the symmetry center of the chain.

where $R$ is the distance to the symmetry center of the chain measured on the CCD. The parameter $D_0 = 2.45 \pm 0.01$ is the demagnification near the symmetry center and $D_2 = -(1.55 \pm 0.08)\ \mathrm{cm}^{-2}$ is the quadratic distortion term. According to this formula the demagnification in the outer region of the II chain differs roughly 20% from the value at the symmetry center.

At the exit of the third II stage a CCD matrix [#3] is coupled by a fiber taper to the chain to convert the optical signal in an electrical one. The matrix consists of 550 lines with 288 photosensitive pixels each. The active pixel area is $12 \times 23\ \mu\mathrm{m}^2$ and the line pitch is 16 μm. There is a nonphotosensitive pixel array of the same size which is used as memory. The shift of one image into the memory zone can be realized within 120 μs. The readout time for the memory zone is 20 ms. A fast clear of the image zone can be achieved in 1 μs.

The raw video signal is transported to a special image processing port (IPP) [#4] which converts the analogue pixel content into digital values. Before being digitised the IPP allows an analogue subtraction of the noise level and an amplification of the remaining signal. For the resulting 8-bit pixel amplitudes a threshold cut can be applied and only pixels with an amplitude above this threshold are transfered to the output. A toolset of on-line programs is available to perform a more complicated data filtering on the IPP level [12] using a 68030 based processor [#5].

## 4. The silicon microstrip detector telescope

Each of the five paddles of the telescope contains a pair of silicon strip detectors (SSD) measuring the two coordinates in a plane perpendicular to the beam. The active area of the upstream paddles is $3.2 \times 3.2\ \mathrm{cm}^2$ whereas the downstream paddles have a size of $6.4 \times 6.4\ \mathrm{cm}^2$ each. The thickness of the silicon wafers is 280 μm. The diode strip pitch is 25 μm but relying on charge divison the readout pitch is chosen to be 100 μm.

The individual silicon wafers are adjusted with a microscope relative to one edge of the paddle with a precision of 5 μm. To ensure that the strips of all detectors measuring the $x(y)$ coordinate are parallel the horizontal edges of the detector frames were adjusted using a clinometer with a scale unit of 20 μm per 1 m length. The paddles are roughly aligned to each other by a groove in the steel bench, the precise final alignment was done by reconstructed beam tracks. The longitudinal positions of the paddles were measured to an accuracy of 100 μm using a micrometer screw. Periodically, a few thousand triggers were recorded to check the alignment of the paddles and the stability of their positions during data taking.

The first step of the analysis is the search for hits from minimum ionizing particles (mip) in each detector. The hit finding is confronted with the fact that each channel has an individual pedestal superimposed on a fluctuating base level of the whole detector. Hence, we subtract first from the raw data the mean pulse height calculated for each detector and then correct the pulse height for the pedestal of each channel.

The charge generated by a traversing particle should mainly be collected from the two readout strips closest to the particle track. A small signal can also be induced in the next but one readout strip [13]. Therefore, we are looking for clusters of at most three neighbouring strips. Only strips with a signal greater than $1\sigma$ of the pedestal fluctuation, which correspond roughly to 10% of the signal of a mip, were accepted for the clustering. A threshold of $4\sigma$ was chosen for the total cluster pulse height to define a hit. For one detector the signal-to-noise ratio of accepted track hits is shown in

[#3] TH 7864, Thomson-CSF, 38 rue Vauthier BP305 F-92102 Boulogne-Billancourt CEDEX, France.

[#4] ELTEC GmbH, D-4200 Mainz, Galileo Galilei Str. 11, Germany.

[#5] FIC 8232, CES, Route du Pont-Butin 70, Petit-Lancy 1, Geneva, Switzerland

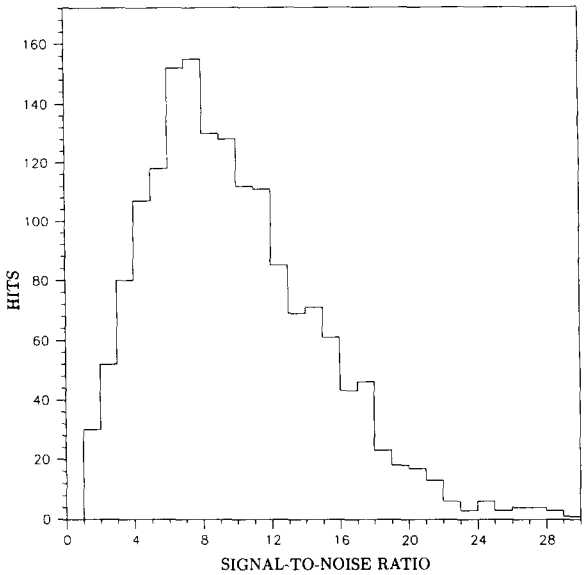


Fig. 5. The signal-to-noise ratio of hits from a minimum ionizing particle in a silicon microstrip detector. For the track fit only hits with a signal greater than $4\sigma$ were accepted.

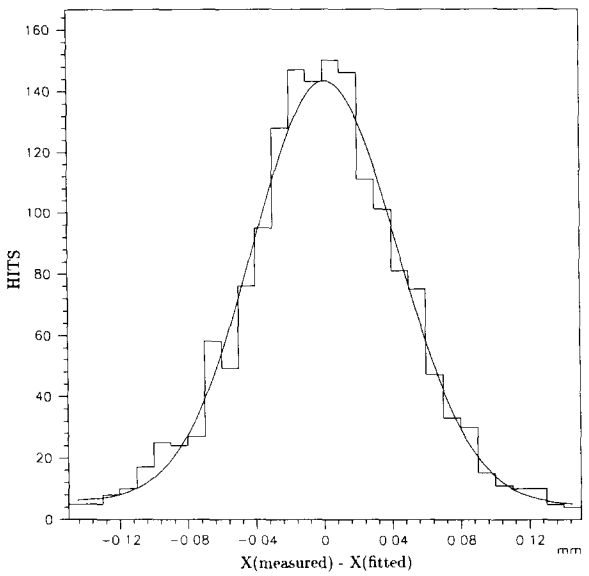


Fig. 6. The distance between hit coordinates and the fitted beam track in a silicon microstrip detector. The curve is a Gaussian with a standard deviation of 42 μm above a constant background term.

fig. 5. The corresponding mean values for all detectors are summarized in table 1.

The hit coordinate, an estimate of the position where the particle traversed the detector, was calculated by the center of gravity method. The resolution was determined in a special laboratory setup of three precisely parallel and closely packed silicon detectors using cosmic muons with an energy above 0.5 GeV. After unfolding the multiple Coulomb scattering contribution a resolution of 12 μm was obtained. This value is in good agreement with the theoretical prediction from the model of capacitive charge division [13] and compatible with results for a similar silicon detector used in the ALEPH experiment [14].

About 30% of all clusters have a signal from only one readout strip. This can happen if the particle traverses the detector very close to this strip or because of a badly working channel. The latter case results of course in a deterioration of the resolution. The fraction of clusters with a signal from three readout strips is on the average less than 3%. The average strip multiplicity for all detectors is given in table 1.

The reconstruction of the beam tracks is based on the four paddles measuring the $x$ and $y$ coordinates. Taking into account that not all channels were working properly, the multiplicity of hits in a paddle should be less than 1 if a beam particle traverses the telescope without interacting. The average multiplicity was found typically between 1.0 and 1.5 indicating that some noise clusters survive the threshold cut of $4\sigma$ for the total cluster pulse height. The idea was not to loose too many track clusters by hard selection criteria because there are at maximum four hits per track projection. At least three hits per projection were required for an accepted beam track.

A distribution of the distance between the measured coordinate in one of the detectors and the reconstructed track is shown in fig. 6. The standard deviations are typically between 40 and 50 μm for all

Table 1
Characteristics of the silicon microstrip detectors: for each detector of the 5 paddles the mean values of the signal-to-noise ratio for hits, the number of strips per hit, the fraction of bad channels over the full detector size and the detection efficiency for hits from beam tracks are given

| Detector | Signal-to-noise ratio | Strip multiplicity | % fraction of bad channels | % hit efficiency |
|---|---|---|---|---|
| 1$x$ | 8.7 | 1.7 | 11.6 | 91.8 |
| 1$y$ | 10.1 | 1.6 | 19.1 | 80.9 |
| 2$x$ | 8.9 | 1.7 | 27.3 [a] | 85.7 |
| 2$y$ | 9.9 | 1.7 | 11.2 | 76.9 |
| 3$x$ | 8.0 | 1.5 | 19.3 | 51.7 |
| 3$y$ | 10.6 | 1.6 | 13.3 | 90.6 |
| 4$u$ | 9.1 | 1.7 | 10.0 | 59.6 |
| 4$u$ | 11.0 | 1.8 | 14.1 | 70.1 |
| 5$x$ | 7.9 | 1.8 | 1.8 | 83.4 |
| 5$y$ | 10.3 | 1.6 | 25.5 | 86.1 |

[a] 20% of the bad channels results from a dead CAMEX-chip.

detectors. The main contribution to the track residual is the multiple Coulomb scattering in the SSD paddles, in the trigger scintillators and in the fiber target. From a Monte Carlo simulation of a 5 GeV $\pi^-$ beam passing the setup we found that the contribution of multiple scattering amounts to 35 μm, only slightly varying with the position of the paddles and the thickness of the fiber targets which were used [15]. By comparison of the measured track residuals with the contribution from multiple scattering and the internal SSD resolution we conclude that the misalignment of the paddles is less than 10 μm.

The inefficiency of a SSD paddle results from badly working channels. These were either physically disconnected or excluded by software because their pulse heights show an abnormal behaviour. The latter happens more often while the number of really dead channels amounts typically to 1% of the total. As can be seen from table 1, the total inefficiency varies strongly between different paddles from 2% up to 25%. These values represent the inefficiencies over the full size of the paddles. For the recorded beam tracks only the efficiency over the effective beam profile, which is defined by the size of the trigger scintillators, is of importance. Analysing reconstructed beam tracks, the average detection efficiency in a paddle was found to be ~80%. The values for all paddles are given in table 1.

Finally, using the hit and track finding algorithm as described above the data from the SSD telescope allows 45% of the $x$–$z$ projections and 58% of the $y$–$z$ projections of all beam tracks to be reconstructed. The combination of both projections were found for 27% of the events.

## 5. Trigger and data acquisition

The trigger system consisted of four scintillation counters equipped with 1 in. photomultipliers [16]. Two crossed scintillation counters downstream and upstream of the fiber target defined an effective beam profile of $5 \times 5$ mm$^2$. A large scintillation counter following the SSD telescope and matching roughly the active SSD area separates interacting from noninteracting beam tracks. By discrimination of small signals from this counter the fraction of interactions in the fiber target can be enhanced.

The readout of the SSD telescope is controlled by a special electronic module. Based on an internal clock sequence, a 1 μs long time interval is provided during which the detectors are active, while sampling and reset amounts to 2.5 μs. This SSD control module is also used to synchronize the readout of SSD and CCD data. It starts the fast clear of the CCD 1.1 μs before the SSDs are activated, so that both systems are ready for data taking at the same time.

For the subsequent data acquisition a VME based OS/9 system with SPIDER as process manager was used [17]. The SPIDER kernel consists of parallel tasks which have access to a common storage area, the circular buffer. This buffer has a storage capacity of 32 kbytes. Communication between the readout electronics and the SPIDER system is done by a CAMAC STATUS-A register [18]. The data transfer to the SPIDER circular buffer was initiated when a trigger signal was arising during a particle burst. The readout and multiplexing of the SSD data was realized by ac-coupled CAMEX 64A chips [19] mounted close to the silicon wafers. Their analog signals were converted by CAMAC FADCs of 1024 channels each of 6 bits capacity. It takes about 2.5 ms to transfer the FADC data into the SPIDER circular buffer. The CCD data were read from the memory of the IPP module. Depending on the threshold cut of the pixel amplitude one has to transfer a few 100 bytes up to about 300 kbytes to an external mass storage. When the event size exceeded 32 kbytes, the physical events were written as more than one logical event. The data were written in the standard EPIO format onto cartridge during the interburst period [20].

## 6. Results of methodical investigations

In this section we analyse the data of two typical runs to demonstrate the capabilities of the setup. We begin with the data from a coherent fiber bundle consisting of round plastic fibers of 500 μm diameter [#6]. It has a cross section of $10 \times 20$ mm$^2$ and was exposed to the beam in a distance of 15 cm to the first II entrance window. We studied the characteristics of the light spots on the CCD pixel array which result from photoelectrons of the first II photocathode. These spots are normally much larger than the pixel size. Therefore one has to cluster all pixels of a spot finding the center of such a cluster which provides the information where the initial photon has hit the photocathode of the first II.

We continued with data from a bundle of cylindrical glass capillaries of 100 μm diameter [#7] filled with NE209D [#8]. The bundle has a hexagonal shape of 10 mm maximum diameter and the beam crossed the target at a distance of 10 cm from the II chain. The

[#6] SCSF38 plastic scintillator, Kuraray Co. Ltd., Tokyo, Japan.
[#7] Schott Fiber Optics Inc., Southbridge, MA, USA
[#8] Isopropyl-Biphenyl (IBP) doped with 0.015 mol/l 1-Phenyl-3-Mesityl-2-Pyrazoline (PMP).

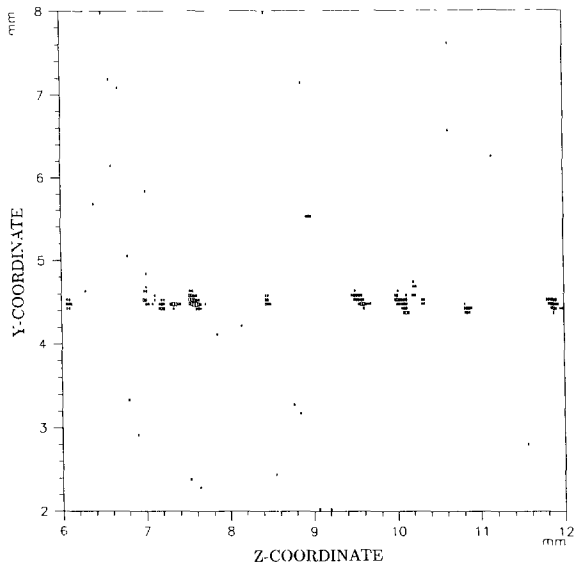


Fig. 7. A part of a CCD pixel image showing photoelectron spots from a charged particle traversing the target made of 500 μm plastic fibers. The scale corresponds to the entrance window of the image intensifier chain.

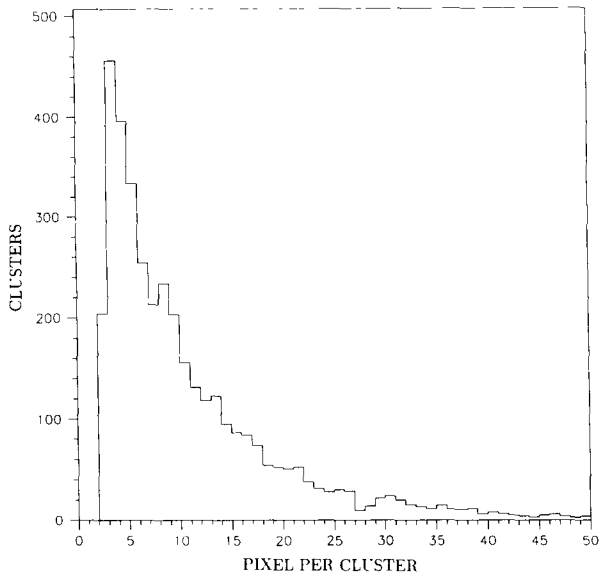


Fig. 8. The background corrected multiplicity of photoelectron spots. Only spots with one local maximum were accepted. The contribution of noise clusters was calculated from a region outside the target.

resolution of the II chain was optimized for readout of fibers of this size.

The tracks of charged particles traversing a bundle of scintillating fibers should be visible as a sequence of pixel clusters on the CCD. Clusters inside a track road of a given width were supposed to originate from a charged particle. The characteristics of clusters inside and outside the track road were used to separate fiber light spots from accidental combinations of noise pixels. Finally, the hit densities were calculated using either CCD data only and using additional track information from the SSD telescope.

In the first step of the off-line analysis it was attempted to attribute the accepted pixels to common clusters. A window of the pixel array with a part of a track in the 500 μm plastic fiber bundle is shown in fig. 7. As one can see, single photoelectron spots of a characteristic size are visible. We used data of the 500 μm fibers to study this spot size because the probability that spots of photons from different fibers overlap is small. Nevertheless all clusters were checked for more than one local maximum by increasing the software threshold for the pixel amplitude. To exclude overlapping spots only clusters with one local maximum were accepted. The background corrected distribution of the pixel multiplicity for single photoelectron clusters is shown in fig. 8. A maximum at three pixels per cluster is found. Because of the long tail of the distribution the average value is 10 pixels per cluster. To exclude the noise clusters we accepted in further analysis only clusters with at least three pixels. The loss of track clusters due to this cut is less than 5%.

The cluster size limits the two-track resolution of a fiber detector. The projection of the cluster profile,

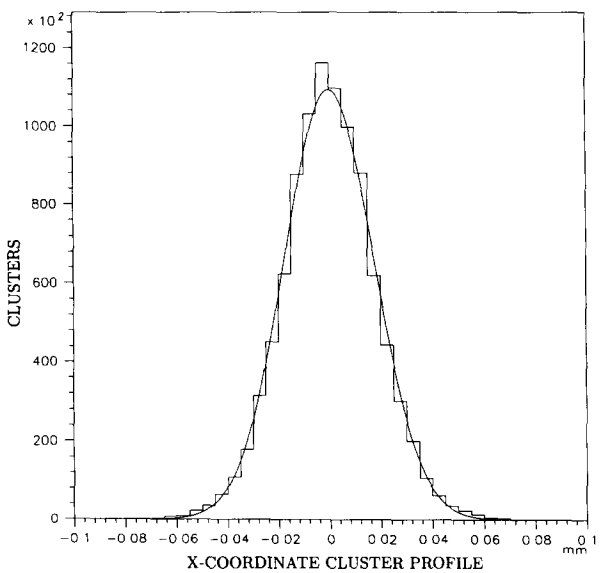


Fig. 9. The projection of cluster profiles on the CCD: distances between the cluster center of gravity and the pixel centers. The shape can be well described by a Gaussian with a standard deviation of 18 μm.

determined from the dependence of the pixel amplitude on the distance to the cluster center of gravity is shown in fig. 9. The distribution can be well described by a Gaussian with a standard deviation of 18 μm. The width is mainly determined by the intrinsic spatial resolution of the second and third stage of the II chain. To obtain the two-track resolution of the fiber detector the demagnification of the II chain is still to be taken into account. For the parametrization of the demagnification as given in section 3 the two-track resolution near to the center of the II chain is ~ 90 μm.

Next, we analysed the data of the 100 μm capillary bundle. We repeated the study of the cluster characteristics for this target and found good agreement with the results of the 500 μm plastic fiber target. The spot size of one photoelectron depends only on the resolution of the II chain and not on the fiber parameters.

An important parameter of a fiber detector is the hit density, i.e. the number of track clusters per unit track length. Before applying a straight line fit to the data the geometrical distortion of the fiber coordinates was corrected as described in section 3. Using an iterative procedure, the cluster with the farthest distance to the fitted line is removed until all clusters are inside a track road of $\pm 3\sigma$ around the fitted track. At least three clusters inside the road are required to accept a track. The value $\sigma$ was determined from the residual distribution of the track clusters shown in fig. 10. Fitting a Gaussian with a constant background term

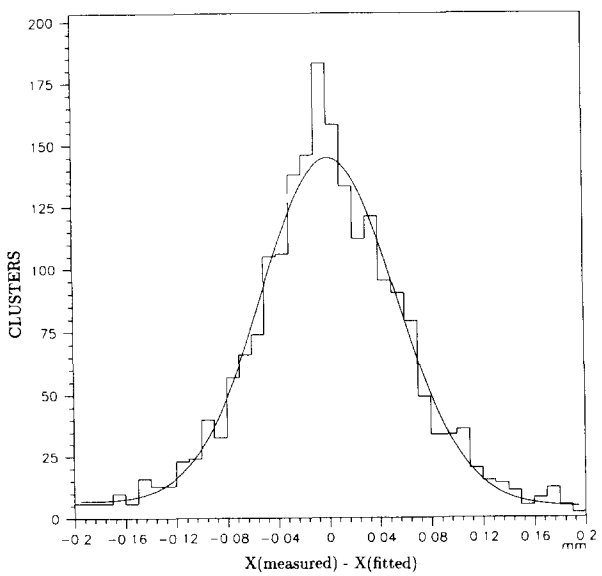


Fig. 10. The distances between the CCD cluster centers and the fitted beam track. The fit takes into account all clusters inside a track road of $\pm 3\sigma$. The distribution is parametrized by a Gaussian of 52 μm standard deviation above a constant background term.

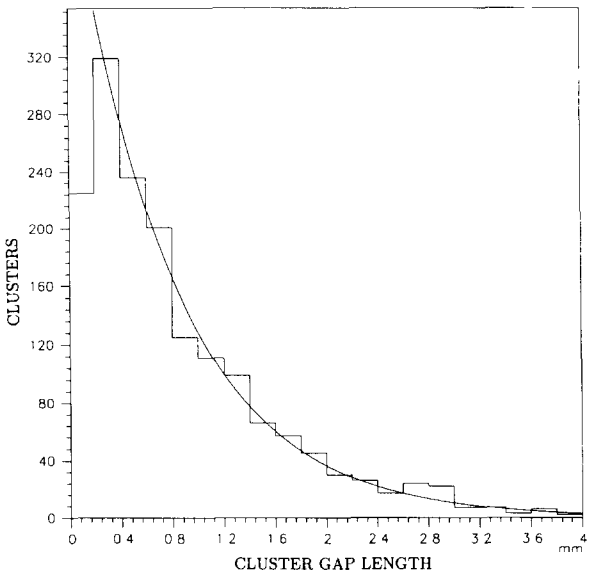


Fig. 11. The gap length between neighbouring CCD clusters from tracks in the 100 μm capillary target in 10 cm distance to the II chain. The distribution can be described by an exponential curve with a slope of 1.28 $mm^{-1}$. The first bin was excluded from the fit

yields $\sigma = 52$ μm. The nonzero background level shows that also some noise cluster with three or more pixels exist. The value $\sigma$ describes the spatial resolution of the fiber target detector. The main contributions are the dispersion of the photons inside a fiber, the spatial resolution of the II chain and a possible incoherency of the fiber target.

The hit density can be derived from the distribution of gap length between adjacent track clusters. The average gap length is inversely proportional to the hit density. For beam tracks passing the 100 μm capillary target in 10 cm distance to the II chain, this distribution is shown in fig. 11. About 20% of the track clusters have more than one local maximum. The corresponding loss of clusters can be seen in the first bin of the gap length distribution. To calculate the average gap length we fit an exponential function to the gap length distribution with exclusion of the first bin [21]. From the fitted slope we derive an average hit density of 1.28 $mm^{-1}$.

However, tracks with a small number of hits cannot be found using only CCD data. Also the fraction of events with a correctly reconstructed beam track is not well known.

The aim of the SSD telescope is to have a precise external reference for beam tracks. In this way one can reduce the above mentioned uncertainties of measurements with the II chain. First, one has to find a common coordinate system for both detector systems.

Again, as for the alignment of the SSD telescope itself, beam tracks were used for this purpose. Applying a rotation and a shift the differences of the corresponding track parameters in the SSD telescope and the CCD pixel array were minimized. In the following analysis we accept only events with a reconstructed beam track traversing the fiber target. About 50% of all triggers have such a track in the projection which is seen by the II chain.

To measure the accuracy of the track prediction from the SSD telescope we calculate the distances between the CCD cluster coordinates and the SSD track. The resulting distribution is shown in fig. 12. It can be described by a Gaussian of 205 μm standard deviation. This value results from the resolution of the SSD telescope, the resolution of the II chain with the fiber target, and the deviation due to Coulomb scattering in the fiber target and the nearby trigger counters. The SSD telescope is not very sensitive to scattering in the target region because the paddles are arranged in two groups downstream and upstream of the target. Taking into account that the SSDs measure the coordinates of beam tracks with an accuracy of 40–50 μm and the average residual of CCD cluster coordinates of 50 μm, then the main uncertainty of the SSD track prediction is again caused by multiple scattering.

To study the influence of multiple scattering on the SSD track reconstruction we have simulated the test run conditions using a Monte Carlo program [15]. At 5 GeV/$c$ beam momentum the Coulomb scattering contributes 160 μm, which is to be compared with the measured value of ~ 200 μm for the average distance between SSD track and CCD clusters. For a precision

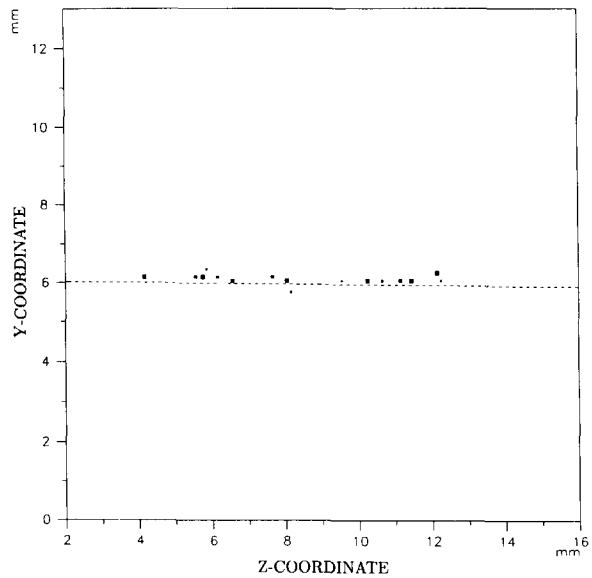


Fig. 13. An event image of the 100 μm hexagonal capillary bundle. The centers of all pixel clusters weighted by their total pulse height and the beam track (dashed line) predicted by the silicon microstrip telescope are shown. All dimensions are in real space without demagnification.

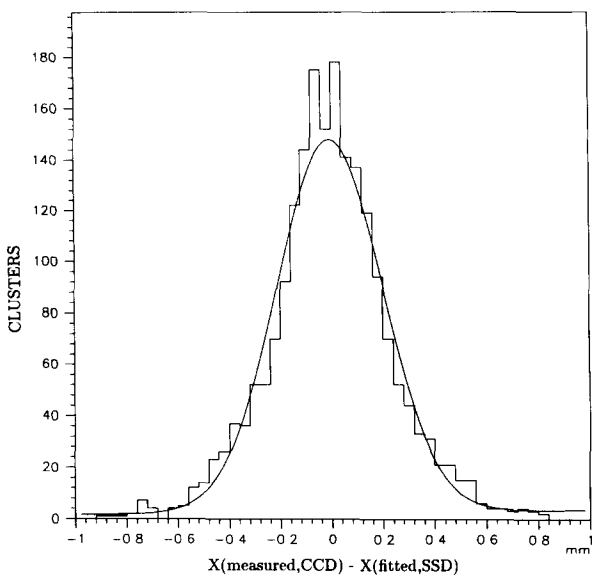


Fig. 12. Distances between the CCD track cluster coordinates and the beam track reconstructed from the hits of the silicon microstrip detector telescope. The shape is described by a Gaussian of 205 μm standard deviation above a linear background term.

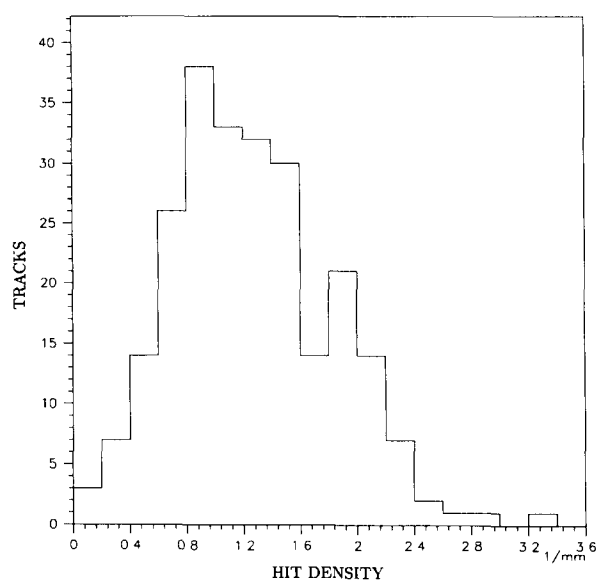


Fig. 14. The hit density of beam tracks. The number of pixel clusters in the region predicted by the silicon microstrip telescope was divided by the total track length in the bundle. The contribution of overlapping cluster is taken into account by the multiplicity of local cluster maxima.

of 50 μm or better a particle beam with an energy above 20 GeV is necessary.

Finally, we calculate the hit density for beam tracks traversing the fiber target. The pixel clusters inside a road of ±500 μm around the SSD track, about 2.5σ of the resolution, were counted as the beam track. A track image in the hexagonally shaped target is shown in fig. 13 together with the reconstructed beam track from the SSD telescope. Dividing the multiplicity of track clusters by the total track length inside the fiber target we obtain an average hit density of 1.25 $mm^{-1}$. The corresponding distribution of the hit density is shown in fig. 14. Although the hit density is in good agreement with the value from the gap length method, the track samples are quite different. For the data sample under consideration, the SSD telescope indicates 244 beam tracks passing through the fiber bundle, but only 130 of them can be recognized using CCD data alone. The lost CCD tracks have either a too small number of hits or are not identical with the triggered beam tracks. The latter can happen if the phosphor screen still emits light from a particle which passed the target shortly before the trigger signal. This demonstrates the need of an external reference system which ensures unbiased measurements of scintillating fiber parameters.

## 7. Summary

A test beam setup for systematic studies of scintillating fiber bundles or ribbons was built. First methodical results from two different targets, made of 500 μm plastic fibers and 100 μm capillaries filled with the liquid scintillator NE209D respectively, exposed to a 5 GeV $\pi^-$ beam of the CERN-PS were discussed.

The main components of the detector system are a scanner bench where the fiber targets are coupled to a three stage image intensifier chain and a silicon microstrip detector telescope.

The silicon microstrip telescope consisting of five two-dimensional detectors is used as an external reference system for the fiber measurements. The mean efficiency to find a hit of a beam particle in a single detector was about 80%. For about one half of all events a beam track in the fiber target can be predicted.

The analysis of the CCD data relies on the spot size of single photoelectrons. Using a cluster algorithm for adjacent pixels we found the value of 35 μm for the full width at half maximum of the cluster profile on the CCD. Taking into account the demagnification this value results in a two-track resolution of 90 μm at the center of the II chain.

After alignment of the SSD and CCD coordinate systems we found that beam tracks in the fiber target can be predicted with a precision of ~200 μm. The main contribution to this value comes from the multiple Coulomb scattering in the SSDs and the fiber target.

Using the SSD track information we obtained for the 100 μm capillary bundle a hit density of ~1.3 $mm^{-1}$ for beam particles crossing the target in 10 cm distance from the readout chain. In comparison with measurements without external reference system this value is free from uncertainties due to unknown loss of tracks.

The first runs were mainly devoted to test the readout scheme of the image intensifier chain in combination with a silicon microstrip telescope. To obtain larger hit densities, as already measured for similar fiber targets [22], a further optimization of the critical readout parameters is necessary. The setup has been shown to be an effective device for investigations of small diameter scintillating fiber targets and ribbons.

## Acknowledgements

We gratefully acknowledge the help of J. Dupont, J. Dupraz and P. Nappey in preparation of the targets and the optoelectronic readout chain. We are also indebted to Y. Perrin and L. Tremblet for their constructive co-operation in the adaptation of the new SPIDER version for the DAQ system. During the data taking we were supported by M. Luban, P. Maksimovic, C. Michotte, E. Peesen and F. Pille. Finally we acknowledge fruitful discussions with G. Zacek, V. Zacek and many other colleagues of the CHORUS collaboration.

## References

[1] G. Jarlskog and D. Rein (eds.), Proc. Large Hadron Collider Workshop, Aachen, 1990, CERN 90-10.
[2] R. Nahnhauer (ed.), Proc. Workshop on Application of Scintillating Fibers in Particle Physics, Blossin, 1990.
[3] K. Winter, Acta Phys. Hungaria 68 (1990) 135;
R. Nahnhauer and V. Zacek, CERN-PPE/90-138 (1990).
[4] C. d'Ambrosio et al., Proc. Large Hadron Collider Workshop, Aachen, 1990, eds. G. Jarlskog and D. Rein, vol. 3, S. 255.
[5] R. Ansorge et al., Nucl. Instr. and Meth. A265 (1988) 33
[6] D. Acosta et al., Nucl. Instr. and Meth. A308 (1991) 481 and Nucl. Instr. and Meth. A302 (1991) 36.
[7] A. Artamonov et al., Nucl. Instr. and Meth. A300 (1991) 53;
J. Bähr et al., Nucl. Instr. and Meth. A306 (1991) 169.
[8] M. Adinolfi et al., CERN-PPE/91-66.
[9] S.V. Golovkin et al., Nucl. Instr. and Meth. A305 (1991) 385.

[10] C. d'Ambrosio et al., CERN-PPE/91-72.
[11] A.D. Bross et al., Nucl. Instr. and Meth. A307 (1991) 35.
[12] ELTEC Electronic, Mainz, Technical Specifications.
[13] U. Kötz et al., Nucl. Instr. and Meth. A235 (1985) 481.
[14] W. Buttler et al., Nucl. Instr. and Meth. A273 (1988) 778; C. Batignani et al., CERN PRE 90-071.
[15] R. Brun et al., CERN - DD/EE/84-1.
[16] A description of the photomultiplier FEU84 can be found in: V.N. Evdokimov et al., IHEP preprint 86-34 (1986).
[17] SPIDER User's Guide, version 4, CERN DD Division OC Group, 1989; A. Bischoff et al., CHORUS-Internal Report 92 - 11 (1992).
[18] CAMAC-Standard: e.g. CERN CAMAC notes.
[19] CAMEX - chip, see also ref. [14].
[20] H. Grote and I. McLaren, CERN I101 EPIO, 1981/1989.
[21] P. Lendermann, Dipomarbeit, Ludwig- Maximilians-Universität München, 1991.
[22] N.S. Bamburov et al., Nucl. Instr. and Meth. A289 (1990); C. Angelini et al., Nucl. Instr. and Meth. A254 (1987) 500.